

MIT Open Access Articles

*Dichotomous parvalbumin interneuron populations
in dorsolateral and dorsomedial striatum*

The MIT Faculty has made this article openly available. **Please share**
how this access benefits you. Your story matters.

Citation: Monteiro, Patricia et al. "Dichotomous parvalbumin interneuron populations in dorsolateral and dorsomedial striatum." *Journal of Physiology* (August 2018): 3695-3707 © 2018 The Authors and The Physiological Society

As Published: <http://dx.doi.org/10.1113/jp275936>

Publisher: Wiley

Persistent URL: <https://hdl.handle.net/1721.1/126428>

Version: Author's final manuscript: final author's manuscript post peer review, without publisher's formatting or copy editing

Terms of use: Creative Commons Attribution-Noncommercial-Share Alike



DOI: 10.1113/JP275936

Dichotomous parvalbumin interneuron populations in dorsolateral and dorsomedial striatum

Patricia Monteiro^{1,2,3,4}, Boaz Barak¹, Yang Zhou¹, Rebecca McRae¹, Diana Rodrigues⁴, Ian R. Wickersham¹ and Guoping Feng^{1,2}

¹McGovern Institute for Brain Research, Department of Brain and Cognitive Sciences; Massachusetts Institute of Technology; Cambridge, MA, 02139; USA

²Stanley Center for Psychiatric Research; Broad Institute of MIT and Harvard; Cambridge, MA, 02139; USA

³PhD Programme in Experimental Biology and Biomedicine (PDBEB), Center for Neuroscience and Cell Biology; University of Coimbra; Coimbra, 3004; Portugal

⁴Life and Health Sciences Research Institute (ICVS), School of Medicine, University of Minho and ICVS/3B's - PT Government Associate Laboratory, Braga/Guimarães, 4710-057; Portugal

Conflict of Interest: the authors declare no competing financial interests.

Author contribution:

Patricia Monteiro: Conception or design of the work; Acquisition or analysis or interpretation of data for the work; Drafting the work or revising it critically for important intellectual content; Final approval of the version to be published; Agreement to be accountable for all aspects of the work; Boaz Barak: Acquisition or analysis or interpretation of data for the work; Final approval of the version to be published; Agreement to be accountable for all aspects of the work; Yang Zhou: Acquisition or analysis or interpretation of data for the work; Final approval of the version to be published; Agreement to be accountable for all aspects of the work; Rebecca McRae: Acquisition or analysis or interpretation of data for the work; Final approval of the version to be published; Agreement to be accountable for all aspects of the work; Ian R. Wickersham: Acquisition or analysis or interpretation of data for the work; Final approval of the version to be published; Agreement to be accountable for all aspects of the work; Guoping Feng: Conception or design of the work; Acquisition or analysis or interpretation of data for the work; Drafting the work or revising it critically for important intellectual content; Final approval of the version to be published; Agreement to be accountable for all aspects of the work.

This is an Accepted Article that has been peer-reviewed and approved for publication in the The Journal of Physiology, but has yet to undergo copy-editing and proof correction. Please cite this article as an 'Accepted Article'; [doi: 10.1113/JP275936](https://doi.org/10.1113/JP275936).

This article is protected by copyright. All rights reserved.

Funding:

This work was funded by the Stanley Center for Psychiatric Research at the Broad Institute of MIT and Harvard and a doctoral fellowship from the Portuguese Foundation for Science and Technology to P.M. (SFRH/BD/33894/2009). Research in the Laboratory of Guoping Feng related to this project has been supported by the Poitras Center for Affective Disorders Research at MIT, Stanley Center for Psychiatric Research at Broad Institute of MIT and Harvard, National Institute of Health (NIMH R01MH097104), Nancy Lurie Marks Family Foundation, and the Simons Foundation Autism Research Initiative (SFARI). B.B. was supported by postdoctoral fellowships from the Simons Center for the Social Brain at MIT and the Autism Science Foundation and is currently a faculty at The School of Psychological Sciences and Sagol School of Neuroscience, Tel Aviv University, Israel. P.M. is currently supported by Society in Science, The Branco Weiss Fellowship, administered by Eidgenössische Technische Hochschule (ETH) Zürich, and European Molecular Biology Organization (EMBO) Long-Term Fellowship (ALTF 89–2016).

Acknowledgements:

We thank Triana Dalia, Sarah Schneck and Heather Sullivan for technical support and all Feng lab members for helpful discussion, especially Holly Robertson, Qiangge Zhang and Dongqing Wang. P.M. would like to thank Prof. Nuno Sousa and Fernanda Marques (ICVS, UMinho, Portugal), Prof. Carlos Duarte (UCoimbra, Portugal), and to acknowledge the support from “Programa Doutoral em Biologia Experimental e Biomedicina” (CNC, Coimbra, Portugal).

Running title: Parvalbumin interneurons in dorsal striatum

Corresponding author - Name: Guoping Feng

Corresponding author - Address:

McGovern Institute for Brain Research
Department of Brain and Cognitive Sciences
Massachusetts Institute of Technology
MIT, 46-3143A

43 Vassar Street
Cambridge, MA 02139

Corresponding author - Phone: 617-715-4898; 617-715-4920

Corresponding author - Fax: 617 324-6752

Corresponding author - E-mail address: fengg@mit.edu

Keywords: Parvalbumin, Fast spiking interneurons, Striatum

Key points summary:

- Existence of two electrophysiological dichotomous populations of parvalbumin (PV) interneurons located in the dorsal striatum.
- Striatal PV interneurons in medial and lateral regions significantly differ in their intrinsic excitability.
- Parvalbumin interneurons in dorsomedial striatum, but not dorsolateral striatum, receive afferent glutamatergic input from cingulate cortex.

Dichotomous parvalbumin interneuron populations in dorsolateral and dorsomedial striatum

ABSTRACT

Dorsomedial striatum circuitry is involved in goal-directed actions or movements that upon repetition become habits, encoded by dorsolateral striatum. An inability to shift from habits can compromise action-control and prevent behavioral adaptation. But although these regions seem to be clearly behaviorally distinct, little is known about their distinct physiology.

Parvalbumin (PV) interneurons are a major source of striatal inhibition and are usually considered as a homogeneous population in the entire dorsal striatum. Here, we recorded PV interneurons in dorsal striatum slices from WT male mice and suggest the existence of two electrophysiological dichotomous populations. We found that PV interneurons located at the dorsomedial striatum region have increased intrinsic excitability as compared to PV interneurons in dorsolateral region. We also found that PV interneurons in dorsomedial region, but not dorsolateral striatum region, receive short-latency excitatory inputs from cingulate cortex. Therefore, our results demonstrate the importance of considering region specific parvalbumin interneuron populations when studying dorsal striatal function.

INTRODUCTION

Daily goal-directed actions often become habitual automated responses after consecutive repetition (Yin and Knowlton, 2004; Yin et al., 2004, 2005, 2006; Hilário and Costa, 2008; Baldan Ramsey et al., 2011; Hilario et al., 2012). Striatum function is crucial for this habit-formation and for proper psychomotor behavior such as motor control, procedural learning and behavioral switching (Yin and Knowlton, 2006; Hilário and Costa, 2008; Steiner and Tseng, 2010; Parent, 2012). Adult striatum dysfunction results in loss of action-control (Graybiel, 2008) and its dysfunction has recently been linked to OCD and ASD (Ahmari et

al., 2013; Burguière et al., 2014; Monteiro and Feng, 2015, 2017; Ahmari, 2016), thickening the list of previously known classic striatum-related disorders such as Parkinson and Huntington's disease (Kreitzer and Malenka, 2008; Plotkin and Surmeier, 2015).

Parvalbumin (PV) interneurons are critical circuit modulators and are thought to be malleable throughout life in the adult brain (Plotkin et al., 2005; Kepecs and Fishell, 2014; Dehorter et al., 2015). In rodent striatum, PV interneurons represent only a small neuronal percentage (~1%) but provide prominent feedforward inhibition to medium-spiny projection neurons (MSNs) (Tepper et al., 2008; Gittis et al., 2010). Decreased numbers of striatal PV interneurons, but not MSNs, have been reported in post-mortem caudate and putamen tissue from patients with Tourette syndrome, suggesting a link between action-control and interneuron pathology in specific striatum sub-regions (Kataoka et al., 2010; Xu et al., 2015, 2016). In rodents, DMS and DLS regions are part of an homogeneous structure, lacking the anatomical segregation between caudate and putamen regions seen in primates (Reep et al., 2003; Voorn et al., 2004). However, PV expression, is more abundant laterally than medially in rodents (Kita et al., 1990; Todtenkopf et al., 2004). Given this anatomical segregation of PV expression, we asked whether striatum PV interneurons could be electrophysiologically different in DLS versus DMS regions. Our data provides the first evidence of dichotomous physiological properties between PV interneurons located in the two striatum regions.

MATERIALS AND METHODS

Ethical Approval

All animal procedures were reviewed and approved by the MIT Committee on Animal Care (CAC). Only male mice were used for experiments. Detailed methods are described below.

Experimental animals

PV-Cre mice (*Pvalb*^{tm1(cre)Arbr}) were purchased from the Jackson Laboratory (JAX Stock No:008069) and ROSA26-stop^{flox}-tdTomato cKI mice were gently provided by Dr. Fan Wang (Duke University School of Medicine). Both mouse lines have been previously described (Hippenmeyer et al., 2005; Arenkiel et al., 2011). Specific primers were designed in this study to distinguish PV-cre heterozygous from homozygous mice:

Primer 5'-GCTCAGAGCCTCCATTCCCT-3'

Primer 5'-GCTCAGAGCCTCCATTCCCT-3'

Primer 5'-CAGCCTCTGTTCCACATACTTC-3'

ROSA26-stopflox-tdTomato^{+/+} mice were crossed with PV-Cre mice to generate PV-Cre^{+/-}:ROSA26-stopflox-tdTomato^{+/+} mice for electrophysiology recordings. Animals were housed on controlled environment (12h light/dark cycles, 24h temperature and humidity monitoring), 2-5 mice *per cage* and *ad libitum* food and water. All experimental procedures were reviewed and approved by the MIT Committee on Animal Care (CAC).

Slice preparation

Acute striatal slices were prepared from 6-8-week-old PV-cre^{+/-}:ROSA26-stopflox-tdTomato^{+/+}. Animals were anesthetized by avertin intraperitoneal injection (tribromoethanol, 20 mg/ml, 0.5 mg/g body weight) and transcardially perfused with cutting NMDG-based aCSF (mM): 92 N-methyl-D-glucamine (NMDG), 2.5 KCl, 1.20 NaH₂PO₄, 30 NaHCO₃, 20 HEPES, 25 glucose, 2 thiourea, 5 Na-ascorbate, 3 Na-pyruvate, 0.5 CaCl₂·2H₂O, 10 MgSO₄·7H₂O (~300 mOsm, 7.2-7.4 pH) (Ting et al., 2014). Following decapitation, brain was removed and coronal brain slices (300 μm) were prepared using a Vibratome 1000 Plus (Leica Microsystems, USA). Slices were recovered in cutting solution at 32–34°C for 10-15 minutes and transferred to room-temperature carbogenated regular aCSF (mM): 119 NaCl, 2.5 KCl, 1.2 NaH₂PO₄, 24 NaHCO₃, 12.5 glucose, 2 MgSO₄·7H₂O,

2 CaCl₂·2H₂O (~300 mOsm, 7.2-7.4 pH). All slices were allowed to recover at least ≥1h prior to whole-cell recordings.

Electrophysiology recordings

Slices were transferred to the recording chamber (RC-27L, Warner Instruments) and constantly perfused with carbogenated regular aCSF at 30±2°C, ~2 ml/minute rate. Borosilicate glass microelectrodes (King Precision Glass) were pulled on a P-97 horizontal puller (Sutter Instruments) and backfilled either with KGlu, CsCl or CsGlu internal (KGlu mM: 145 K-Gluconate, 10 HEPES, 1 EGTA, 2 MgATP, 0.3 NaGTP and 2 MgCl₂; pH adjusted to 7.3 with KOH and osmolarity adjusted to ~300 mOsm with sucrose. CsGlu mM: 110 CsOH, 110 D-Gluconic acid, 15 KCl, 4 NaCl, 5 TEA-Cl, 20 HEPES, 0.2 EGTA, 5 Lidocaine N-ethyl chloride, 4 MgATP, 0.3 NaGTP; pH adjusted to 7.3 with KOH and osmolarity adjusted to ~300 mOsm with K₂SO₄. CsCl mM: 103 CsCl, 12 CsOH, 12 Methanesulfonic acid, 5 TEA-Cl, 10 HEPES, 0.5 EGTA, 5 Lidocaine N-ethyl chloride, 4 MgATP, 0.3 NaGTP, 10 Phosphocreatine, 4 NaCl; pH adjusted to 7.3 with KOH and osmolarity adjusted to ~300 mOsm with K₂SO₄), presenting a typical resistance around 2-4 MΩ.

Slices were visualized under IR-DIC (infrared-differential interference contrast) using a BX-51WI microscope (Olympus) and recordings were obtained after seal rupture and internal equilibrium from visually identified *td*Tomato-positive cells. All recordings were always obtained in parallel for both cell populations (DLS-PV and DMS-PV) along the lateral-medial striatal axis within each brain slice. Only the DLS region close to the corpus callosum and DMS close to the lateral ventricles, were targeted for recordings to avoid any potential “intermediate” region. Input resistance was obtained through extrapolation from the I-V plot as well as direct measurement through -150pA hyperpolarizing current step.

Picrotoxin 100 μ M and TTX 1 μ M were added for mEPSC experiments and AP-V 50 μ M, NBQX 10 μ M and TTX 1 μ M were added for mIPSC experiments (all drugs from Tocris). Striatal EPSCs and EPSPs were evoked by a 0.1ms stimulation step (Isoflex, AMPI) delivered at 0.05Hz frequency by a platinum iridium concentric bipolar electrode (CBAPC75, FHC) placed in cingulate cortex layers 4/5 (stimulation electrode 1-1.5mm away; stimulation intensity ranged from 0.1 to 3.0mA). Latency was measured as the time between the stimulation (electrode artifact) and the onset of the resulting EPSC. EPSPs and action potential (AP) graphically displayed traces were obtained at -50 mV by gradual increasing stimulation intensity until AP firing. Stimulation artifacts were partly removed for clarity of the EPSP figure. Summary EPSP data (onset time, peak, rise and decay time) were extracted from the largest evoked EPSP at -70 mV from pairs of PV-MSN adjacently located (same stimulation electrode location and intensity for each PV-MSN pair). Analysis of EPSCs and EPSPs was performed on averaged responses from 3-5 sweeps. PV cells were identified based on *tdTomato* signal and all presented hyperpolarized resting membrane potential (~ -85 mV) and typical AP-shape upon current-injection. Putative MSNs were identified based on soma size (12-20 μ m), absence of *tdTomato* signal, typical hyperpolarized resting membrane potential (~ -85 mV) and typical AP-shape upon current-injection. EPSP rise time was measured from 10% to 90% of the peak amplitude of the synaptic response. Decay time was measured by a single exponential fit. Onset of Cg-evoked DMS-EPSPs was measured as the delay between the stimulus delivery and the EPSP foot. Data was acquired using a MultiClamp 700B amplifier and a Digidata 1440A. Signals were filtered at 1-2 KHz and digitized at 10 KHz. For current-clamp recordings, bridge balance was adjusted and pipette capacitance neutralized. Series resistance compensation (<20 M Ω) was performed in voltage-clamping mode. Theoretical liquid junction potential was estimated to be around -11 mV and not corrected-for.

Antibodies

Mouse and rabbit anti-parvalbumin antibodies (PV235 and PV27, 1:5000 dilution) from Swant; mouse anti-DARPP32 (611520, 1:1000) from BD Biosciences; rabbit anti-Somatostatin (AB5494, 1:200) from Millipore; rabbit anti-Neuropeptide Y (T-4070, 1:250) from Peninsula Laboratories International; goat anti-ChAT antibody (AB144P, 1:500 dilution) from Millipore; chicken anti-GFP (ab13970, 1:5000) from Abcam.

Morphological experiments and quantification of PV immunoreactivity

For morphological experiments Biocytin (0.3-0.5% w/v) was included in KGlu internal solution during patch clamp recordings. Recorded slices were fixed in 4 % PFA (paraformaldehyde), kept in 4 % PFA overnight at 4 °C, and then transferred to PBS. Next day slices were incubated for 2h in AlexaFluor-488 streptavidin conjugate (1:1000, Invitrogen), washed 3x in PBS and mounted for imaging. For TSA-immunohistochemistry, rabbit anti-parvalbumin antibody (Swant, PV27) was used together with Tyramide signal amplification (TSA) (Invitrogen, T-20922) according to TSA kit instructions. Quantification of PV-immunoreactivity was performed using cellSens imaging software (Olympus).

IHC and microscope imaging

Mice were anesthetized by isoflurane inhalation and transcardially perfused with PBS solution followed by 4 % PFA (paraformaldehyde) fixative solution. Brains were kept in 4 % PFA overnight at 4 °C, then transferred to PBS and sectioned at 50 microns. Sections were washed 3x in PBS and permeabilized for 5 minutes using a PBS solution containing 10% MeOH, 3% H₂O₂, and 0.5% NaBH₂, except for ChAT immunostaining and virus experiments. Slices were again washed 3x PBS and incubated in 1.2 % Triton-X 100 for 15

minutes, followed by another 3x PBS wash. Blocking was then performed for 1h in PBS containing 2% BSA and 0.2% Triton-X. Primary antibodies were incubated overnight at 4°C for detection of the respective antigens. Next day sections were washed 3x PBS, followed by 2-4h incubation with secondary antibody (species-specific Alexa-conjugated antibody, 1:1500, Invitrogen) at room temperature. Lastly, sections were washed 3x PBS, stained for DAPI, mounted in ProlongGold (Invitrogen) or Fluoro-Gel (Electron Microscopy Sciences) and imaged using Olympus Fluoview FV1000 confocal and Olympus BX61 microscopes. Serial sections were reconstructed as 3D models using BioVis3D software (<http://www.biovis3d.com/>, Montevideo, Uruguay).

Surgeries and viruses

6-8 weeks old mice were anesthetized with isoflurane, placed on a stereotactic frame and viral injections performed using a Nanoject device (Drummond scientific). For monosynaptic tracing experiments we injected ~0.2 μ l of undiluted AAV2/8-synP-DIO-sT-P2A-EGFP-P2A-B19G (2.29e12 gc/ml [gc = genome copies]) at DLS or DMS (bregma coordinates for guide cannula implantation: DLS ML+2.75, AP+0.5, 2.0; DMS ML+2.0, AP+0.5, 2.3; please note that the injector/infusion cannula further extends 1mm DV). 2-3 weeks later we injected ~0.2 μ l of undiluted RV- Δ G-RFP(EnvA) (titer 2.75E9 i.u./ml [i.u. = infectious units]) at the same bregma location. All stereotaxic coordinates are from bregma/skull. Mice were sacrificed 7days later to observe expression pattern. AAV-synP-DIO-sTpEpG and RV Δ G-RFP(EnvA) were generated by I.R.W. from MIT Genetic Neuroengineering Group (Massachusetts Institute of Technology) (Kohara et al., 2014).

Experimental Design and Statistical Analysis

All statistical analyses were performed using Prism (GraphPad Software) and MATLAB Software (MathWorks). Non-normal distributions were assumed for all the datasets regardless of variance and sample size. Pairwise comparisons were performed using Mann Whitney test for unpaired data and Wilcoxon Signed Rank test for paired data comparisons, with a threshold of $p < 0.05$ for significance. All datasets are presented as means \pm s.e.m. Further details on particular analyses can also be found on the respective figures/results section and Table 1.

RESULTS

To study dorsal striatum PV interneurons, we started by crossing PV-*Cre* mice with ROSA26-stop^{fllox}-*tdTomato* reporter mice, to fluorescently label PV interneurons for cell-targeted patch clamp recordings. Immunostaining of PV-*Cre*:*tdTomato*⁺ striatal brain sections, showed faithful colocalization between *tdTomato* signal and PV immunostaining, indicating successful *tdTomato* expression under the control of endogenous PV promoter (Fig. 1). To further confirm correct PV interneurons labeling by this strategy, we also performed separate immunostaining protocols with other well-known striatal markers. Colocalization was not observed between *tdTomato* native signal and immunostaining for other striatal markers such as DARPP32, SOM, NPY, or ChAT, indicating a correct reporting strategy (Fig. 1).

We next examined passive and active membrane properties by performing whole-cell intracellular electrophysiology. Recordings from PV interneurons located in DMS and DLS regions showed that these populations markedly differed in intrinsic excitability (Fig. 2A-E and Table1). PV located in DMS showed higher intrinsic excitability, as represented by their leftshifted I-V curve (Fig. 2A). Input resistance obtained through extrapolation from the I-V

plot as well as direct measurement through a -150 pA hyperpolarizing current step, showed significantly higher values for DMS-PV than DLS-PV (Fig. 2B) (DMS-PV mean= 43 M Ω ; DLS-PV mean= 28 M Ω). In addition, significantly higher membrane resistance was observed for the DMS population (Fig. 2B) (DMS-PV mean= 118 M Ω ; DLS-PV mean= 85 M Ω). Active membrane properties also showed that DMS-PV interneurons are more excitable, displaying a left-shifted I-F curve (Fig. 2C). Action potential triggering (rheobase) also required less current injection compared to DLS-PV population (DMS-PV mean= 424 pA; DLS-PV mean= 584 pA) (Fig. 2D). Resting membrane potential (DMS-PV= -86 mV; DLS-PV= -85 mV) and spike threshold (DMS-PV mean= -39 mV; DLS-PV mean= -41 mV; Fig. 2E) were not different between the two populations, and thus do not seem to contribute for the observed excitability differences.

But because differences in excitability can also arise from differences in membrane surface area, we measured whole-cell capacitance (roughly proportional to membrane surface area). Capacitance recordings confirmed smaller values for DMS-PV than DLS-PV (Fig. 2F), suggesting that the differences in excitability could be attributable, at least in part, to different membrane areas.

To explore if these differences in electrophysiology could accompany differences in morphology, we acquired morphological data from DMS-PV and DLS-PV by using TSA-enhanced parvalbumin immunostaining (Fig. 3) and by using biocytin-filled patch pipettes during electrophysiology recordings. We found that DLS-PV consistently displayed more extensive arborization and complexity than DMS-PV interneurons. This morphological observation supports whole-cell capacitance measurements, which indicated larger capacitance values for DLS-PV than DMS-PV. Quantification of PV-immunoreactivity also showed stronger detection in the more lateral regions of the striatum compared to DMS (Fig.3).

We next investigated striatal synaptic connectivity for both PV populations. Significantly higher mEPSC frequency was observed in DMS-PV interneurons as compared to DLS-PV interneurons, with no significant differences in amplitude (Fig. 2G and Table1). In addition, DMS-PV received significantly fewer inhibitory synapses than DLS-PV, with no differences in amplitude (Fig. 2H and Table1). These results could suggest the existence of two discrete PV populations with functional differences in synaptic connectivity. Given that local synapses within the striatum are inhibitory, the mEPSC frequency data suggested that either DMS-PV received more excitatory inputs from a shared afferent source with DLS-PV, or that DMS-PV received inputs from an afferent source distinct from DLS-PV.

To resolve this question at the cellular level, we decided to generate modified pseudotyped rabies-virus and performed for the first time *in vivo* *Cre*-dependent monosynaptic retrograde tracing specifically from striatal PV interneurons.

First, a conditional helper virus (AAV-synP-DIO-sTpEpG) was injected either into DMS or DLS region of PV-*Cre* mice. After *Cre*-mediated recombination, this AAV helper virus expressed EGFP and two proteins: TVA (receptor for the avian EnvA, necessary for subsequent rabies virus infection) and B19G (the rabies glycoprotein necessary for monosynaptic retrograde spreading) (Wall et al., 2010). Then, two weeks post injection, modified EnvA- Δ G-RFP-rabies-virus (EnvA-pseudotyped, G-deleted, RFP-rabies) was injected into the same location, allowing monosynaptic retrograde tracing from striatum PV interneurons (Fig. 4A).

Histological analysis revealed that DMS-PV interneurons receive dense afferent innervation from cingulate cortex (Cg) (Movie 1 and Fig. 4B,C,F, Fig. 5A-C). This cortical projection was not observed for PV interneurons in DLS region (Movie 2 and Fig. 4D,E,G). Both populations of PV interneurons in DMS and DLS seemed to integrate histological inputs from thalamus and GP regions.

To functionally test this identified cortical-DMS-PV projection, we placed a stimulation electrode in deep-layer Cg and recorded post-synaptic evoked responses from DMS region. Given that PV interneurons in DLS do not receive inputs from Cg, we compared DMS PV interneurons with neighboring MSN-*tdTomato* negative neurons.

Stimulation of cingulate cortex evoked a reliable glutamatergic excitatory response in both DMS-MSN neurons and DMS-PV interneurons (Fig. 5D-E and Table1). The average latency of cortical-evoked DMS-EPSCs was significantly shorter in PV interneurons than DMS-MSNs, indicating a rapid cortical recruitment of striatal inhibition (Fig. 5D-E and Table1). Cortical-evoked subthreshold DMS-EPSPs had a trend for faster onset time and trend for larger amplitude in DMS-PV interneurons compared to neighboring DMS-MSNs (Fig. 5F-G and Table1). Rise time was not significantly different between MSN and PV interneurons, although DMS-EPSPs decay time had a trend for slower in MSNs (Fig. 5H-I and Table1). These observations indicated that DMS-PV interneurons are strongly enervated by cingulate cortex and cortical inputs may affect PV interneurons more strongly than MSN neurons, potentially allowing PV interneurons to control the recruitment and spread of second messengers more efficiently in the striatum. Moreover, these findings demonstrate for the first time that, similar to medium-spiny neurons, PV interneurons also receive glutamatergic inputs from distinct cortical regions along the medial-lateral axis of the striatum.

DISCUSSION

Our findings demonstrate the existence of two dichotomous PV interneuron populations along the medial-lateral axis of the dorsal striatum. Whole-cell recordings revealed that DMS-PV interneurons have more excitable intrinsic membrane properties as compared to PV interneurons in dorsolateral region. Given the important role of the DMS region during initial behavioral learning (Yin et al., 2005; Ragozzino, 2007), having a more excitable PV population in this region could provide means for efficient behavioral inhibition

during an initial ‘trial-and-error’ learning phase. In a scenario where an unexpected outcome occurs and behavioral flexibility is required (*e.g.* early learning phase), a more excitable PV population, such as the DMS-PV population, could therefore be more easily triggered and inhibit/shape local MSNs firing to promote behavioral adaptation. On the other hand, once a task has been extensively repeated and a specific behavioral strategy has proven to be effective, it should be preserved and not easily changed (habitual behavior; DLS-mediated). In this second habitual scenario, stronger inputs would thus be needed to activate the less excitable DLS-PV interneurons and stop an ongoing habitual response.

Moreover, the fact that associative Cg inputs specifically target DMS-PV interneurons, but not PV interneurons in dorsolateral striatum, further suggests that these discrete PV populations in lateral and medial territories are part of distinct corticostriatal networks and may in fact contribute to the hypothesized parallel/competing roles of DLS and DMS in controlling behavior (Hilario et al., 2012). Our data provide the first evidence of dichotomous physiological properties between PV interneurons along the medial-lateral axis of the dorsal striatum, and highlight the importance of considering region specific parvalbumin interneuron populations when studying the dorsal striatum.

REFERENCES

- Ahmari SE (2016) Using mice to model Obsessive Compulsive Disorder: From genes to circuits. *Neuroscience* 321:121–137.
- Ahmari SE, Spellman T, Douglass NL, Kheirbek M a, Simpson HB, Deisseroth K, Gordon J a, Hen R (2013) Repeated cortico-striatal stimulation generates persistent OCD-like behavior. *Science* 340:1234–1239.
- Arenkiel BR, Hasegawa H, Yi JJ, Larsen RS, Wallace ML, Philpot BD, Wang F, Ehlers MD (2011) Activity-induced remodeling of olfactory bulb microcircuits revealed by

monosynaptic tracing. PLoS One 6.

Baldan Ramsey LC, Xu M, Wood N, Pittenger C (2011) Lesions of the dorsomedial striatum disrupt prepulse inhibition. *Neuroscience* 180:222–228.

Burguière E, Monteiro P, Mallet L, Feng G, Graybiel AM (2014) Striatal circuits, habits, and implications for obsessive-compulsive disorder. *Curr Opin Neurobiol* 30C:59–65.

Dehorter N, Ciceri G, Bartolini G, Lim L, del Pino I, Marin O (2015) Tuning of fast-spiking interneuron properties by an activity-dependent transcriptional switch. *Science* (80-) 349:1216–1220.

Gittis AH, Nelson AB, Thwin MT, Palop JJ, Kreitzer AC (2010) Distinct roles of GABAergic interneurons in the regulation of striatal output pathways. *J Neurosci* 30:2223–2234.

Graybiel AM (2008) Habits, rituals, and the evaluative brain. *Annu Rev Neurosci* 31:359–387.

Hilario M, Holloway T, Jin X, Costa RM (2012) Different dorsal striatum circuits mediate action discrimination and action generalization. *Eur J Neurosci* 35:1105–1114.

Hilário MRF, Costa RM (2008) High on habits. *Front Neurosci* 2:208–217.

Hippenmeyer S, Vrieseling E, Sigrist M, Portmann T, Laengle C, Ladle DR, Arber S (2005) A developmental switch in the response of DRG neurons to ETS transcription factor signaling. *PLoS Biol* 3:e159.

Kataoka Y, Kalanithi PSA, Grantz H, Schwartz ML, Saper C, Leckman JF, Vaccarino FM (2010) Decreased number of parvalbumin and cholinergic interneurons in the striatum of individuals with Tourette syndrome. *J Comp Neurol* 518:277–291.

Kepecs A, Fishell G (2014) Interneuron cell types are fit to function. *Nature* 505:318–326.

- Kita H, Kosaka T, Heizmann CW (1990) Parvalbumin-immunoreactive neurons in the rat neostriatum: a light and electron microscopic study. *Brain Res* 536:1–15.
- Kohara K, Pignatelli M, Rivest AJ, Jung H-Y, Kitamura T, Suh J, Frank D, Kajikawa K, Mise N, Obata Y, Wickersham IR, Tonegawa S (2014) Cell type-specific genetic and optogenetic tools reveal hippocampal CA2 circuits. *Nat Neurosci* 17:269–279.
- Kreitzer AC, Malenka RC (2008) Striatal Plasticity and Basal Ganglia Circuit Function. *Neuron* 60:543–554.
- Monteiro P, Feng G (2015) Learning from Animal Models of Obsessive-Compulsive Disorder. *Biol Psychiatry*.
- Monteiro P, Feng G (2017) SHANK proteins: roles at the synapse and in autism spectrum disorder. *Nat Rev Neurosci*.
- Parent A (2012) The History of the Basal Ganglia: The Contribution of Karl Friedrich Burdach. :374–379.
- Plotkin JL, Surmeier DJ (2015) Corticostriatal synaptic adaptations in Huntington’s disease. *Curr Opin Neurobiol* 33:53–62.
- Plotkin JL, Wu N, Chesselet MF, Levine MS (2005) Functional and molecular development of striatal fast-spiking GABAergic interneurons and their cortical inputs. *Eur J Neurosci* 22:1097–1108.
- Ragozzino ME (2007) The contribution of the medial prefrontal cortex, orbitofrontal cortex, and dorsomedial striatum to behavioral flexibility. In: *Annals of the New York Academy of Sciences*, pp 355–375.
- Reep RL, Cheatwood JL, Corwin J V (2003) The associative striatum: organization of cortical projections to the dorsocentral striatum in rats. *J Comp Neurol* 467:271–292.

- Steiner H, Tseng KY eds. (2010) Handbook of Basal Ganglia Structure and Function. Academic Press.
- Tepper JM, Wilson CJ, Koós T (2008) Feedforward and feedback inhibition in neostriatal GABAergic spiny neurons. *Brain Res Rev* 58:272–281.
- Ting JT, Chen Q, Feng G (2011) Improved methods for acute brain slice preparation from adult and aging animals. :2081.
- Todtenkopf MS, Stellar JR, Williams E a, Zahm DS (2004) Differential distribution of parvalbumin immunoreactive neurons in the striatum of cocaine sensitized rats. *Neuroscience* 127:35–42.
- Voorn P, Vanderschuren LJMJ, Groenewegen HJ, Robbins TW, Pennartz CM a (2004) Putting a spin on the dorsal-ventral divide of the striatum. *Trends Neurosci* 27:468–474.
- Wall NR, Wickersham IR, Cetin A, De La Parra M, Callaway EM (2010) Monosynaptic circuit tracing in vivo through Cre-dependent targeting and complementation of modified rabies virus. *Proc Natl Acad Sci U S A* 107:21848–21853.
- Xu M, Kobets A, Du J-C, Lenington J, Li L, Banasr M, Duman RS, Vaccarino FM, DiLeone RJ, Pittenger C (2015) Targeted ablation of cholinergic interneurons in the dorsolateral striatum produces behavioral manifestations of Tourette syndrome. *Proc Natl Acad Sci* 112:893–898.
- Xu M, Li L, Pittenger C (2016) Ablation of fast-spiking interneurons in the dorsal striatum, recapitulating abnormalities seen post-mortem in Tourette syndrome, produces anxiety and elevated grooming. *Neuroscience* 324:321–329.
- Yin HH, Knowlton BJ (2004) Contributions of striatal subregions to place and response learning. *Learn Mem* 11:459–463.

- Yin HH, Knowlton BJ (2006) The role of the basal ganglia in habit formation. *Nat Rev Neurosci* 7:464–476.
- Yin HH, Knowlton BJ, Balleine BW (2004) Lesions of dorsolateral striatum preserve outcome expectancy but disrupt habit formation in instrumental learning. *19*:181–189.
- Yin HH, Knowlton BJ, Balleine BW (2006) Inactivation of dorsolateral striatum enhances sensitivity to changes in the action-outcome contingency in instrumental conditioning. *Behav Brain Res* 166:189–196.
- Yin HH, Ostlund SB, Knowlton BJ, Balleine BW (2005) The role of the dorsomedial striatum in instrumental conditioning. *Eur J Neurosci* 22:513–523.

FIGURES

Figure 1. Native *tdTomato* expression shows faithful colocalization with PV staining in striatal sections from PV-cre:*tdTomato* mice.

Pvalb^{tm1(cre)Arbr}; ROSA26-*stop*^{fllox}-*tdTomato* mice express *tdTomato* fluorescence in striatal parvalbumin interneurons. Fluorescence images of histological sections show colocalization of native *tdTomato* expression (red) with endogenous PV immunoreactivity, but not DARPP32, SOM, NPY or ChAT.

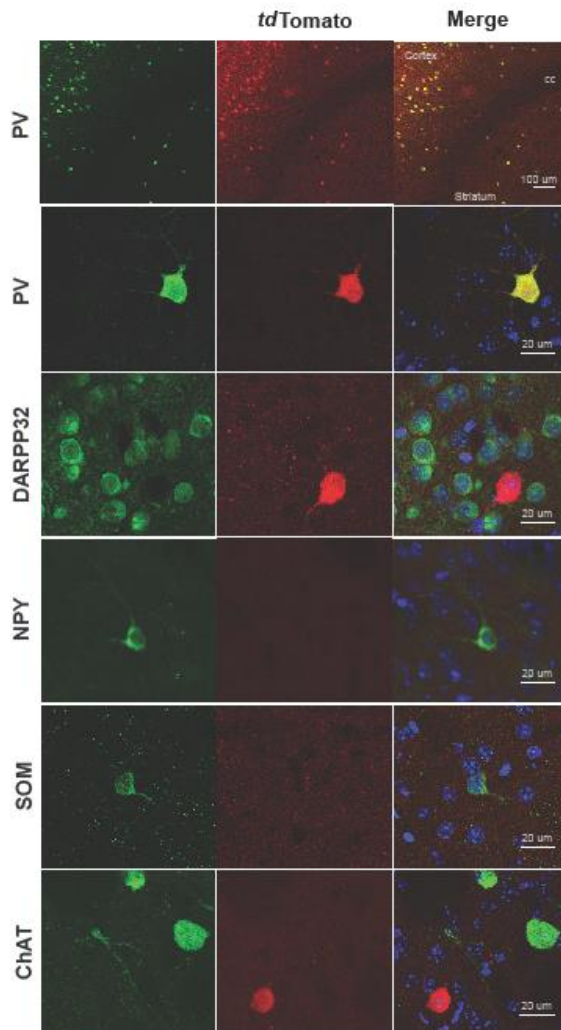


Figure 2. DMS-PV interneurons have distinct intrinsic excitability and synaptic physiology from DLS-PV interneurons.

Higher intrinsic excitability for DMS-PV is shown by their left-shifted IV curve (A) and higher input and membrane resistance (B). (C) IF-plot with representative current injection steps demonstrates increased excitability for DMS-PV interneurons compared to DLS-PV. Please note that the graph only displays current injections up to 740 pA but many DLS-PV required much higher current injections for firing. Given that above 740 pA, many DMS-PV entered in “depolarization blockade” and become inexcitable, the graph is only displayed up to that value.

(D) Lower rheobase current values indicate higher excitability of DMS-PV compared to DLS-PV. (E) No difference in firing threshold. (F) DMS-PV interneurons have smaller capacitance ($p < 0.001$, two-sample Kolmogorov-Smirnov test). (G) Summary bar graphs and cumulative probability curves (200 events *per* interneuron) show significantly increased mEPSC frequency in DMS-PV, with no difference in amplitude. (H) Summary bar graphs and cumulative probability curves (140 events *per* interneuron) show that DMS-PV interneurons have reduced mIPSC frequency; with no difference in amplitude. Example traces are shown at the bottom for G,H. * $p < 0.05$; ** $p < 0.01$; *** $p < 0.001$; All statistical analyses are in Table 1.

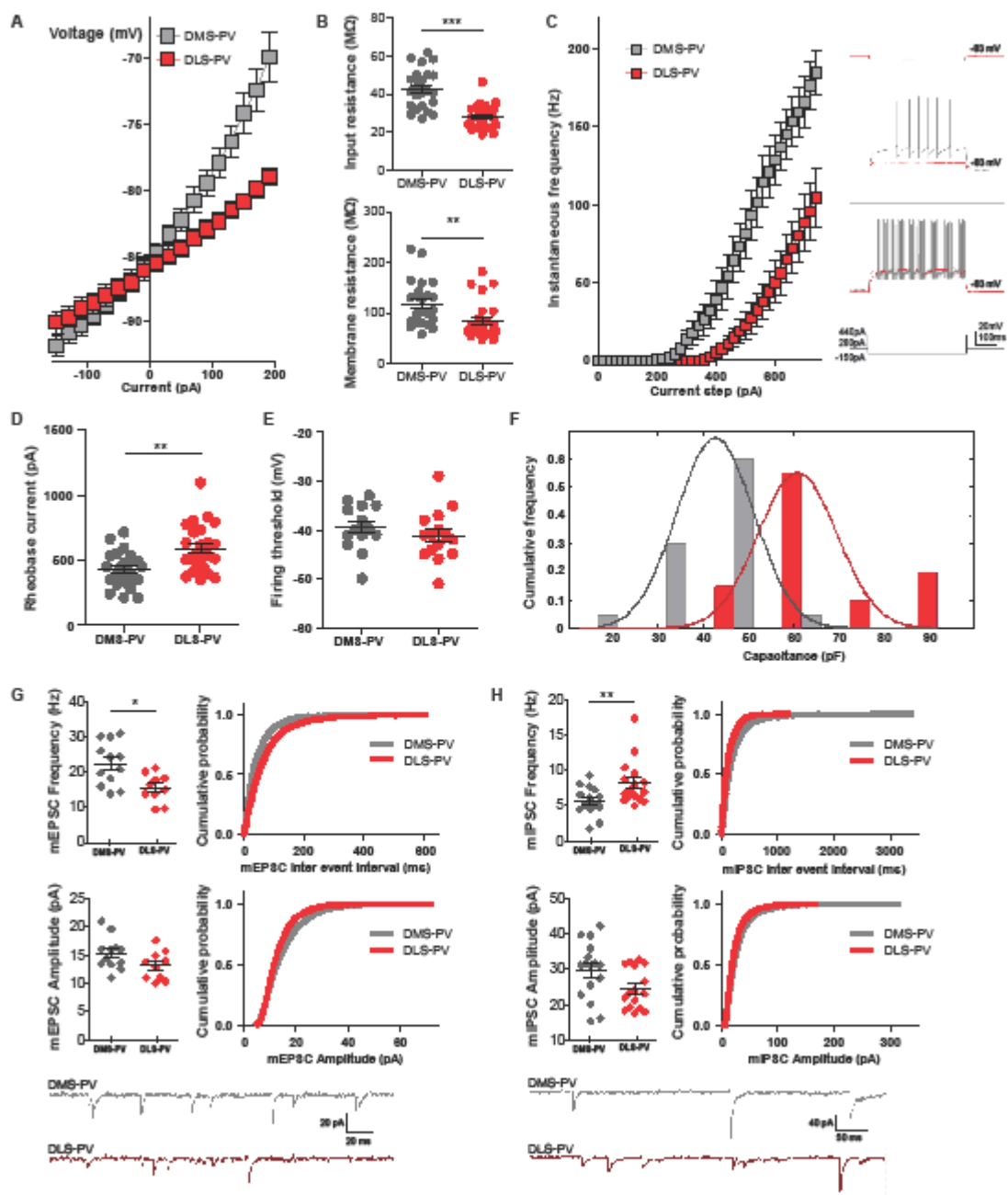


Figure 3. DLS-PV interneurons have more abundant parvalbumin expression and display more complex morphology than DMS-PV.

(A) Parvalbumin interneurons display significantly higher PV intensity *per cell* in dorsolateral striatum compared to dorsomedial striatum ($***p < 0.001$; $n=80$ DLS-PV cells and $n=80$ DMS-PV cells; two-way ANOVA for the left cumulative frequency curves and Kolmogorov–Smirnov test for right histogram distribution). (B) Reconstructed morphology of PV interneurons in DLS (top) and DMS (bottom), after TSA-enhanced parvalbumin immunostaining.

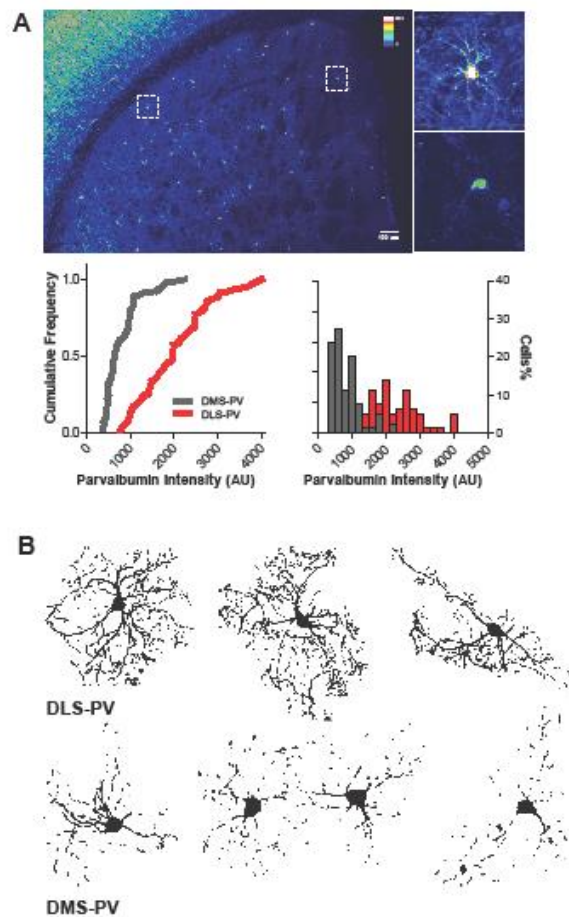


Figure 4. Cre-dependent monosynaptic retrograde tracing from striatum parvalbumin interneurons.

(A) Adult PV-*Cre* mice are injected in the DLS or DMS with AAV expressing TVA, EGFP and rabies glycoprotein (AAV-DIO-sTpEpG) in a *Cre*-dependent manner. Two weeks later, the same mice are injected with EnvA-pseudotyped monosynaptic rabies that can only infect PV interneurons expressing TVA, and can only retrogradely spread from PV interneurons expressing rabies glycoprotein (G). One week after rabies injection, direct inputs onto striatal PV interneurons become labeled (RFP). (B, C, F) DMS-PV interneurons receive dense inputs from cingulate cortex (Cg). RFP labelled Cg-axons can be observed in coronal section. (D, E, G) DLS-PV interneurons receive inputs from motor (M1, M2), somatosensory cortex and from other PV within DLS, but not cingulate cortex (Cg). LO - lateral orbital cortex, FrA - frontal association cortex, PrL - prelimbic cortex, Cg1 - cingulate cortex, area 1, Cg2 - cingulate cortex, area 2, M1 - primary motor cortex, M2 - secondary motor cortex, S1 - primary somatosensory cortex, S2 - secondary somatosensory cortex, RSC - retrosplenial cortex.

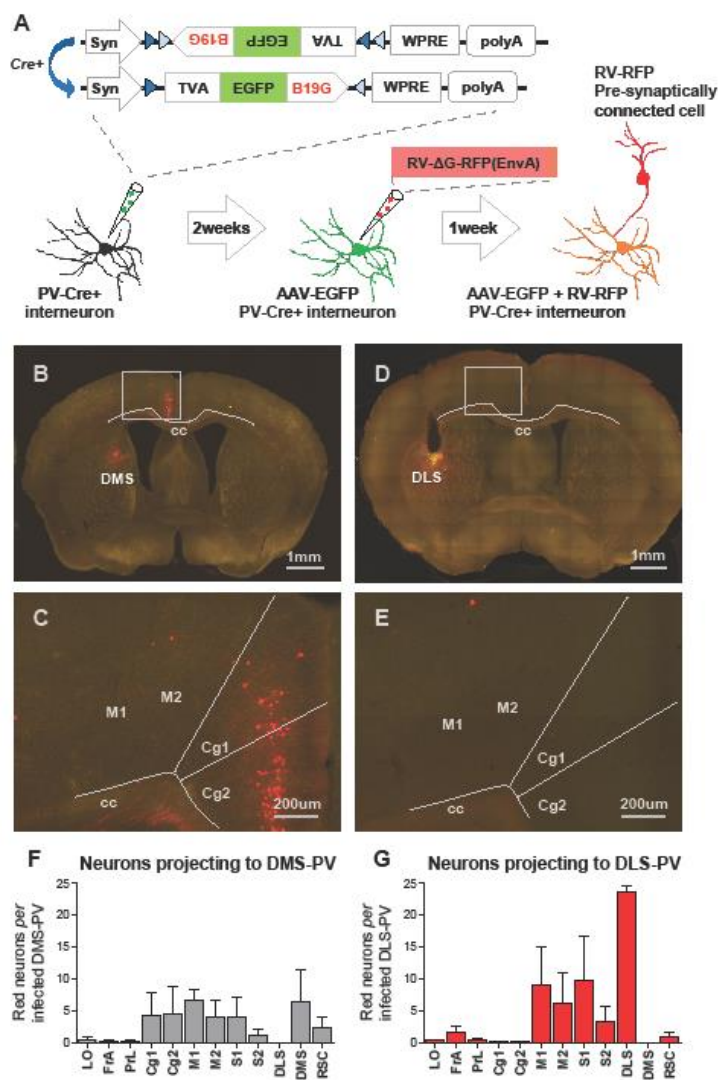
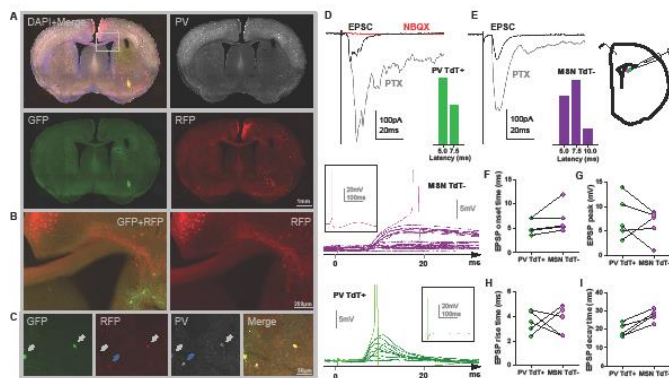


Figure 5. DMS-PV interneurons receive afferent glutamatergic input from Cingulate cortex (Cg).

(A) Cg projection neurons (RFP+) revealed by *Cre*-dependent retrograde monosynaptic labeling from DMS-PV infected interneurons (GFP+). (B) Zoomed image from square area depicted in A; Cg axons (red) projecting to DMS-PV interneurons (green) can be seen in detail. (C) White arrows show DMS-PV interneurons co-infected by AAV-sTpEpG (green) and RV- Δ G-RFP(EnvA) (red); Blue arrow shows a DMS-PV interneuron expressing only RFP, due to rabies retrograde labeling from other synaptically connected PV interneurons. (D, E) Brain slice cartoon and representative traces showing that stimulation of Cg reliably evokes post-synaptic excitatory responses (NBQX-sensitive EPSC) in DMS-PV interneurons and neighboring MSNs; Cumulative distribution of EPSC latency after Cg stimulation shows significantly shorter latencies for DMS-PV interneurons compared to MSNs. (F-I) Summary data extracted from the largest evoked subthreshold EPSP in each pair of PV-interneuron and its respective neighboring-MSN. Representative subthreshold EPSP traces are represented on the left side for both cell types. Each trace results from a gradual increase in the stimulation intensity until action-potential triggering (insets show the full action-potential trace). Statistical analyses are in Table 1.



Movie 1. Cre-dependent monosynaptic retrograde tracing from parvalbumin interneurons in DMS.

3D model reconstructed from serial sections showing afferent cells that project onto dorsomedial striatal PV interneurons.

Movie 2. Cre-dependent monosynaptic retrograde tracing from parvalbumin interneurons in DLS.

3D model reconstructed from serial sections showing afferent cells that project onto dorsolateral striatal PV interneurons.

Table 1. Experimental Design and Statistical Analysis

Figure	Measurement	N	Mean±s.e.m.	Statistical test and P value
Fig.2B (top)	Input resistance (MΩ)	DMS-PV=25 cells	42.76± 2.01	Mann Whitney test, ***p<0.0001
		DLS-PV=25 cells	28.21 ± 1.255	
Fig.2B (bottom)	Membrane resistance (MΩ)	DMS-PV=25 cells	118.1 0± 8.68	Mann Whitney test, **p=0.0013
		DLS-PV=25 cells	84.70 ± 7.44	
Fig. 2D	Rheobase current (pA)	DMS-PV=25 cells	424.4 ± 26.05	Mann Whitney test, **p=0.0019
		DLS-PV=25 cells	583.6 ± 36.17	
Fig. 2E	Firing threshold (mV)	DMS-PV=15 cells	-39.40± 1.17	Mann Whitney test, p=0.1624
		DLS-PV=15 cells	-41.20 ± 1.34	
Fig. 2G	mEPSC Frequency (Hz)	DMS-PV=12 cells	22.31± 1.78	Mann Whitney test, *p=0.0229
		DLS-PV=10 cells	15.49± 1.26	
	mEPSC Amplitude (pA)		15.25 ± 0.83	Mann Whitney test, p=0.1062
		13.08 ± 0.80		
Fig. 2H	mIPSC Frequency (Hz)	DMS-PV=16 cells	5.68 ± 0.49	Mann Whitney test, **p=0.0098
		DLS-PV=16 cells	8.17± 0.79	
	mIPSC Amplitude (pA)		29.66± 2.01	Mann Whitney test, p=0.1011
		24.42 ± 1.43		
Fig. 5D, 5E	EPSC Latency (ms)	DMS-PV=8 cells	5.49± 0.44	Wilcoxon Signed Rank test, *p=0.0156
		DMS-MSN=8 cells	7.04 ± 0.73	
Fig. 5F	EPSP Onset time (ms)	DMS-PV=5 cells	5.42± 0.71	Wilcoxon Signed Rank test, p=0.1250
		DMS-MSN=5 cells	6.88 ± 1.32	
Fig. 5G	EPSP Peak (mV)	DMS-PV=5 cells	7.73± 1.96	Wilcoxon Signed Rank test, p=0.4375

		DMS-MSN=5 cells	6.31 ± 1.43	
Fig. 5H	EPSP Rise time (ms)	DMS-PV=5 cells	3.58 ± 0.41	Wilcoxon Signed Rank test, $p=1.0000$
		DMS-MSN=5 cells	3.67 ± 0.52	
Fig. 5I	EPSP Decay time (ms)	DMS-PV=5 cells	19.22 ± 1.64	Wilcoxon Signed Rank test, $p=0.0625$
		DMS-MSN=5 cells	27.45 ± 1.43	

Patricia Monteiro, PhD, is an EMBO long-term fellow with Prof. Nuno Sousa at the Life and Health Sciences Research Institute (ICVS), School of Medicine, University of Minho, Portugal. She did her PhD work with Prof. Guoping Feng at the Massachusetts Institute of Technology (MIT, USA), where she focused on synaptic and circuitry mechanisms of basal ganglia dysfunction in compulsive and repetitive behaviors. Her current research interests are stress-related disorders, ASD and the role of inhibition in the brain. Patricia is supported by The Branco Weiss Fellowship – Society in Science, administered by Eidgenössische Technische Hochschule (ETH) Zürich, Switzerland.

